Accounting for erroneous electrode data in electrical impedance tomography

Andy Adler

School of Information Technology and Engineering
University of Ottawa, Ontario, Canada
aadler@uottawa.ca

Short Title: Accounting for erroneous electrode data

Keywords: Electrical Impedance Tomography, Image Reconstruction, Electrodes

Corresponding Author: Andy Adler
School of Information Technology and Engineering (*SITE*),
University of Ottawa
800 King Edward ave.
Ottawa, Ontario, Canada, K1N 6N5
Tel: (613) 562-5800 ext. 6218, Fax: (613) 562-5664
Email: aadler@uottawa.ca

Acknowledgements: This work was supported by a grant from the National Science and Engineering Research Council of Canada.

Abstract

An unfortunate occurrence in experimental measurements with electrical impedance tomography, is electrodes which become detached or poorly connected, such that the measured data cannot be used. This paper develops an image reconstruction methodology which allows use of the remaining valid data. A finite element model of the EIT difference imaging forward problem is linearized as z=Hx, where z represents the change in measurements and x the element log conductivity changes. Image reconstruction is represented in terms of a maximum a posteriori (MAP) estimate as $x= \text{inv}(H^t \text{ inv}(R_n) + \text{inv}(R_x)) H^t \text{ inv}(R_n) z$, where R_x and R_n represent the *a priori* estimates of image and measurement noise cross correlations, respectively. Using this formulation, missing electrode data can be naturally modelled as infinite noise on all measurements using the affected electrodes. Simulations indicate position error and resolution are close (±10%) to the values calculated without missing electrode data as long as the target was further than 10% of the medium diameter from the affected electrode. Applications of this technique to experimental data show good results in terms of removing artefacts from images.

Introduction

Electrical Impedance Tomography (EIT) uses body surface electrodes to make measurements from which an image of the conductivity distribution is calculated. Although EIT produces fairly low resolution images, it has some interesting advantages: it is non-invasive, non-cumbersome, and uses potentially low cost electronics components. However, one important difficulty with experimental and clinical EIT measurements is the care required to ensure proper electrode measurements. Typically, eight or sixteen individual electrodes are attached to the patient. However, for more complex applications of EIT the number of electrodes may be even greater, such as for 3D measurements, or the use of separate current stimulation and voltage measurement electrodes. Numerous conditions can cause electrodes to give false readings, especially in long term monitoring applications (Lozano *et al* 1995). Electrodes can become detached, the contact impedance can change because of sweat or peripheral oedema, and changes in subject posture can move electrodes and falsify readings.

Many researchers have investigated sources of inaccuracy in electrode data. Several studies investigated noise and errors due to the electronics hardware. The effect of electronic noise in backprojection image reconstruction was investigated by Frangi *et al* (2002). Measurement errors due to impedance mismatch between cables and the unknown skin-electrode impedance were studied (Al-Hatib, 1998). Meeson *et al* (1996) examined the electronics measurement noise levels in a hospital environment as compared to those more typical to a laboratory. Another line of investigation has considered issues related to electrode application and movement. Lozano *et al* (1995) measured the errors due to electrode replacement and posture change in order to

understand some of the issues in long term EIT measurements. Similarly, Swanson and Webster (1983) investigated errors due to inadequate instrumentation and improper electrode application. The effect of movement of thoracic EIT electrodes during breathing was studied by Adler *et al* (1996b). Another interesting approach was the development of a strategy to apply additional electrodes for impedance pneumography and combine measured values to reduce movement artefacts (Khambete *et al* 2000).

This paper considers the problem of individual electrode errors in EIT. Occasionally, a single electrode will produce invalid data while the other electrodes remain "good". Anecdotal evidence suggests the most common reasons are that the electrode becomes detached or poorly connected, or that there are wiring faults, electronics hardware errors, or problems with the electrode-skin contact. A subject with loose skin is especially prone to the latter effect; our experience with EIT measurements in dogs (with very loose skin) motivates the interest in techniques to deal with these problems. Certain other medical instrumentation techniques, such as electroencephalography (EEG), or electrocardiography (ECG), can also use many electrodes. However, unlike these techniques, EIT imaging algorithms make computations which depend on all electrode data. Thus, a single measurement error impedes calculation of the image. In order to address this problem, an algorithm is proposed which considers erroneous electrode measurements and calculates the conductivity change image using the remaining valid data.

Methods

A methodology is developed to manage reconstruction of EIT difference images from data containing electrode errors. This approach is quite general; it is applicable to any difference image reconstruction algorithm formulated in terms of a regularized inverse based on a Jacobian or sensitivity matrix. In this section, this methodology is described in terms of the algorithm of Adler and Guardo (1996a). Approaches to incorporate this technique into other algorithms are described in the discussion. With respect to terminology, terms *electrode error* and *affected electrode* are taken to be any electrode which produces high noise or unusual or no signal.

Image Reconstruction Formulation

The medium is modelled with a 2D finite element model (FEM) using N first order triangular elements with piecewise constant conductivity. Sixteen electrodes, using point electrode models, are evenly distributed around the medium boundary, and used for current injection and voltage measurement. The FEM, **F** calculates:

$$\mathbf{v} = \mathbf{F}(\boldsymbol{\sigma}) \tag{1}$$

where **v** is an $M\times1$ vector of measured voltages, and **σ** is an $N\times1$ vector of element conductivities.

EIT difference imaging estimates the change in conductivity distribution from a change in measurements. The vector of difference measurements is **z**, where:

$$\mathbf{z}_i = \frac{\mathbf{v}_{\mathbf{a},i} - \mathbf{v}_{\mathbf{b},i}}{\frac{1}{2}\left(\mathbf{v}_{\mathbf{a},i} + \mathbf{v}_{\mathbf{b},i}\right)} \tag{2}$$

where $\mathbf{v}_{\mathbf{a},i}$ is the measured voltage i after a conductivity change, and $\mathbf{v}_{\mathbf{b},i}$ is its value before. For measurements from a saline phantom, $\mathbf{v}_\mathbf{b}$ is typically measured in a homogeneous configuration. The conductivity change image ($\mathbf{x}$) is calculated from the change in element conductivities:

$$\mathbf{x}_i = \log(\boldsymbol{\sigma}_{\mathbf{a},i}) - \log(\boldsymbol{\sigma}_{\mathbf{b},i}) \tag{3}$$

For small changes ($\mathbf{x}$) around a background conductivity level ($\boldsymbol{\sigma}_\mathbf{b}$), the relationship between $\mathbf{x}$ and $\mathbf{z}$ may be linearized as

$$\mathbf{z} = \mathbf{H}\mathbf{x} + \mathbf{n} \tag{4}$$

where $\mathbf{H}$ is the Jacobian, or sensitivity, matrix; it relates a small change in element log conductivities to a change in difference measurements. Noise in the measurement system is represented by $\mathbf{n}$, and assumed to be uncorrelated and Gaussian. Each element i,j of $\mathbf{H}$ is calculated as:

$$\mathbf{H}_{i,j} = \left.\frac{\partial \mathbf{z}_i}{\partial \mathbf{x}_j}\right|_{\boldsymbol{\sigma}_b=\boldsymbol{\sigma}_0} \tag{5}$$

Several authors show details of the calculation of $\mathbf{H}$ from the FEM parameters (e.g. Adler and Guardo (1996a), Polydorides and Lionheart (2002), Vauhkonen *et al* (2001)). $\mathbf{H}$ is calculated at a background conductivity distribution $\boldsymbol{\sigma}_\mathbf{b}=\boldsymbol{\sigma}_0$, which is assumed to be homogeneous.

Image reconstruction is formulated as a linearized, one step estimate, using the maximum a posteriori (MAP) regularization framework; the estimated conductivity change $\hat{\mathbf{x}}$ is calculated:

$$\hat{\mathbf{x}} = \left(\mathbf{H}^t \mathbf{R}_n^{-1} \mathbf{H} + \mathbf{R}_x\right)^{-1} \mathbf{H}^t \mathbf{R}_n^{-1} \mathbf{z} \tag{6}$$

The various parameters are interpreted in term of Bayesian statistics. $\mathbf{R}_x$ is the expected crosscorrelation of image elements, $E[\mathbf{x}\mathbf{x}^t]$. While the calculation of $\mathbf{R}_x$ for our model is described here, the methodology to compensate for electrode errors does not depend on the specific choice of $\mathbf{R}_x$. Diagonal elements of $\mathbf{R}_x$ model the expected range of element log conductivity changes. Off-diagonal values correspond to correlations between image elements; these values will be non zero to because: 1) adjacent regions in the medium tend to undergo similar conductivity changes, and 2) the number of EIT measurements is relatively low, and, as such, does not support image reconstructions with high spatial frequency content. For these reasons, $\mathbf{R}_x$ behaves as a spatial low pass filter. We do not try to model and then invert $\mathbf{R}_x$ directly, but rather model a matrix $\mathbf{Q}$ proportional to $\mathbf{R}_x^{-1}$ as a spatial high pass filter. The high pass cut-off frequency is chosen to correspond to 5% of the medium diameter. $\mathbf{R}_n$ represents the expected crosscorrelation between measurement residuals, $\mathbf{z} - \mathbf{H}\hat{\mathbf{x}}$. In this model, this is the measurement noise, $\mathbf{n}$, and $\mathbf{R}_n$ is $(E[\mathbf{n}\mathbf{n}^t])$. Since noise is uncorrelated between measurements, $\mathbf{R}_n$ is a diagonal matrix, and can be easily inverted to get $\mathbf{W} = \mathbf{R}_n^{-1}$, where $\mathbf{W}_{i,i} = 1/\sigma_i^2$.

In terms of these parameters, the regularized inverse is

$$\hat{\mathbf{x}} = \left(\mathbf{H}^t \mathbf{W} \mathbf{H} + \mu \mathbf{Q}\right)^{-1} \mathbf{H}^t \mathbf{W} \mathbf{z} = \mathbf{B}\left(\mathbf{Q}, \mathbf{W}, \mu\right)\mathbf{z} \tag{7}$$

This is a linear equation, and can be represented by a single reconstruction matrix $\mathbf{B}$ for a given choice of parameters values. Since the relative magnitudes of $\mathbf{R}_n$ and $\mathbf{R}_x$, are unknown, a hyperparameter μ is selected as the ratio of image to noise variance. The value of μ is constrained by the choice of a Noise Figure (NF), defined to be the

ratio of the signal to noise ratio in the image and the signal to noise ratio in the measurements. Thus

$$NF = \left(\frac{E[\hat{\mathbf{x}}]}{var[\hat{\mathbf{x}}]} \right) \Big/ \left(\frac{E[\mathbf{n}]}{var[\mathbf{n}]} \right) \tag{8}$$

Given a user selected NF value, the appropriate μ is calculated using a bisection search technique. Heuristically, a NF of 2 was found to be appropriate for phantom and in vivo data (Guardo *et al*, 1991). All results in this paper use this value of NF.

Electrode Noise Model

We consider an EIT system with N electrodes using bipolar current drive and difference measurements. Voltage values measured on electrodes used for current injection are discarded, but all other measurements are used in the image reconstruction, even though, due to reciprocity (Geselowitz, 1971), only half of these measurements are linearly independent. With no electrode errors there are $N\times(N-3)$ measurements for an adjacent drive current pattern, and $N\times(N-4)$ for other patterns. Electrode errors will further reduce the number of available measurements; for each affected electrode, voltage measurements using that electrode are effected for all current patterns, and all voltage measurements affected for current patterns using that electrode. Figure 1 shows a diagram of the measurements affected by a single electrode error in adjacent drive and opposite drive EIT systems with eight electrodes. The pattern of measurements eliminated due to the measurement configuration forms a diagonal pattern, while electrode errors form vertical and horizontal bands. For an adjacent drive system with a single electrode error, $(N-4)(N-3)$ measurements remain valid, while for a non adjacent drive configuration there will be $(N-4)^2$. For an 8

electrode system this error reduces the number of measurements by 50%, while for a 16 electrode system, the available measurements are reduced by 25%. For a non adjacent drive configuration with a single electrode error, there will be $(N-4)^2$ remaining valid measurements. Certain EIT hardware configurations have electrode error patterns quite different from that shown here. For example, a system using N separate drive and measurement electrodes (e.g. Cook *et al* 1994), will only lose two rows of N measurements for a single measurement electrode error.

Since the signal level in EIT is low, erroneous data will typically dominate the signal, rendering the calculated images unusable. The simplest approach to dealing with this erroneous data is to simply set the problem measurements to zero. This can be represented in the image reconstruction formulation by zeroing each column of the matrix $\mathbf{B}$ corresponding to an affected measurement. This image reconstruction matrix obtained by zeroing erroneous data is referred to as $\mathbf{B}_Z$, while the original (no electrode errors) matrix is $\mathbf{B}_0$. Calculation of $\mathbf{B}_Z$ from $\mathbf{B}_0$ is represented by the following pseudocode:

Set $\mathbf{B}_Z = \mathbf{B}_0$

For each affected measurement i

For $j = 1$ to M

Set $\mathbf{B}_{Z\,j,i} = 0$

While this approach does eliminate the contribution of erroneous data, it introduces distortions to the calculated image, especially if conductivity changes occur near an affected electrode.

A better approach is to explicitly account for errors in the image reconstruction formulation. Fortunately, the presence of electrode errors can be straightforwardly represented in terms of the parameters of the regularized reconstruction algorithm. Electrode errors imply high noise, which is reflected in the measurement noise variance values on the diagonal elements of $\mathbf{R}_n$. Thus, if measurement i is subject to increased noise (by a factor σ_n^2), $\mathbf{W}_{i,i}$ is reduced by the same factor. The reconstruction matrix corresponding to this modified $\mathbf{W}$ is referred to as $\mathbf{B}_{\sigma=\sigma n^2}$. In a scenario where an electrode becomes completely disconnected, or noise levels are very high, σ_n can be assumed to be infinite, and the corresponding elements of $\mathbf{W}$ are $1/\infty=0$. The reconstruction matrix calculated for this noise level is $\mathbf{B}_{\sigma=\infty}$. Calculation of $\mathbf{B}_{\sigma=\sigma n^2}$ is represented by the following pseudocode:

Set $\mathbf{W} = \mathbf{W}_0$

for each affected measurement i

  Set $\mathbf{W}_{i,i} = \mathbf{W}_{0\ i,i} / \sigma_n^2$

Set $\mathbf{B}_{\sigma=\sigma n^2} = (\mathbf{H}^t\mathbf{W}\mathbf{H} + \mu\mathbf{Q})^{-1}\ \mathbf{H}^t\ \mathbf{W}$

Note that, in general, the hyperparameter μ will not be the same for $\mathbf{B}_{\sigma=\sigma n^2}$ and $\mathbf{B}_0$. In each case, μ was selected to obtain an NF of 2.0. The calculated values of μ were approximately 10 percent higher for $\mathbf{B}_{\sigma=\infty}$ for single electrode errors than for $\mathbf{B}_0$.

Test Data

Test data were calculated using a 2D FEM using 1024 triangular elements with 16 compound electrodes distributed evenly on the medium boundary. (This is a different, and larger, model than the FEM used for image reconstruction.) Adjacent and opposite current drive configurations were simulated. Measurements were calculated

for a small (2% of medium diameter) non-conductive contrasting target in an otherwise homogeneous phantom at a sequence of target positions from the centre to the affected electrode. In order to eliminate any possible non-linear interactions between the conductivity contrast and electrode errors, the conductivity changes were chosen to be small; the product of target area and contrast ratio was 10^{-5}. Figure 2 shows reconstructed images of these simulated data, as well as the positions of five simulated electrodes with errors (E_0 to E_4). E_0 is closest to the target, while E_4 is 90° away. The target position was calculated as the centre of mass of the elements in the target and expressed as a fraction of the medium diameter. Thus a target position (x_T, y_T) of (0,0.5) indicates a position halfway between the centre and the top of the medium.

Images were reconstructed of these data using the reconstruction matrices $\mathbf{B}_0$, $\mathbf{B}_Z$, and $\mathbf{B}_{\sigma=\infty}$. Because spatial resolution is non-uniform, EIT systems require specific figures of merit (Wheeler, 2002). For example, for most reconstruction algorithms, the calculated image from a small target has a circular shape only in the centre of the medium, and it becomes more elliptical near the boundary. A classic definition of resolution, such as *full width at half maximum*, is unable to account for such changes in shape. The presence of electrode errors can cause even more unusual reconstructed image shapes. In order to compare the image reconstruction performance of the various reconstruction matrices, the following figure of merit parameters, *position error*, and *resolution* are defined. For each reconstructed image, the reconstructed area, A_R is defined such that it contains 50% of the image amplitude. The reconstructed position (x_R, y_R) is the position of the centre of mass of A_R. Using these values, the figures of merit values are calculated:

$$\textit{position error} = (x_T - x_R\ ,\ y_T - x_R)$$

$$\textit{resolution} = \mathrm{sqrt}(\ A_R / A_0\ )$$

where A_0 is the area of the medium. Details of these calculations are given by Adler and Guardo (1996a).

In order to illustrate this technique with experimental data, results are shown of breathing and lung fluid instillation in dogs. These data were obtained as part of the experiments described by Adler *et al* (1997). Briefly, mongrel dogs were anaesthetized, tracheostomized, and mechanically ventilated. Sixteen ECG-style electrodes for obtaining EIT data were spaced evenly around the shaved thorax 10 cm above the base of the rib cage. An additional three electrodes were attached for recording the ECG. To avoid any contribution from cardiac activity, all EIT data acquisitions were triggered 100 ms after the QRS peak of the ECG. At each tidal volume level, EIT data were acquired at end expiration and end inspiration. Saline solution containing 5% bovine albumin and Evans blue dye was instilled into a lobe of the right lung through a catheter positioned by using a bronchoscope. Volumes of 10, 25, 50, 75, and 100 ml of the fluid were given, and EIT data was acquired at end expiration and end inspiration, after each instillation. Two animals (of nineteen) showed some level of electrode error in the measured data.

Results

Reconstructed images were calculated using the simulated target data illustrated in figure 2, using adjacent and opposite current patterns. Calculations used three reconstruction matrices: 1) $\mathbf{B}_0$ (no electrode errors, top row) 2) $\mathbf{B}_Z$ (electrode error data set to zero, middle row) 3) $\mathbf{B}_{\sigma=\infty}$ (electrode noise in regularized inverse, bottom row). Figure 3 shows the effect of target radial position for an affected electrode E_0. Radial positions of 0, 0.2, 0.4, 0.6, and 0.8, are shown in each column from left to right. For both current patterns, images calculated using $\mathbf{B}_Z$ show significant artefacts for all target positions. As expected, the artefacts increase as the target approaches the affected electrode. Images calculated with $\mathbf{B}_Z$ are better for adjacent drive current patterns than for opposite; the reconstructed target is clearly visible above the image artefacts for target radial positions below 0.6. Reconstructions with $\mathbf{B}_{\sigma=\infty}$ are superior to $\mathbf{B}_Z$. Significant artefacts are only visible at a target positions ≥ 0.8 for adjacent drive current patterns. Interestingly, reconstructed targets near the electrode appear more elliptical for $\mathbf{B}_{\sigma=\infty}$ than $\mathbf{B}_0$. Also, no artefacts are visible for opposite drive; even the "ringing" effect seen with $\mathbf{B}_0$, appears reduced.

In order to quantify the effect of the various reconstruction matrices, position error (figure 4) and resolution (figure 5) are calculated as a function of target position. For both current drive patterns, position error for $\mathbf{B}_Z$ increases roughly linearly with target position, reaching a maximum value above 0.5. This result appears reasonable considering that, once data from E_0 is removed, measurements from the other side of the medium will dominate the image, pushing the reconstructed position away from the affected electrode. Position error for images calculated with $\mathbf{B}_{\sigma=\infty}$ remains low (and close to that for $\mathbf{B}_0$) for all cases, except for adjacent drive for target positions $\geq$

0.7. Images (figure 3A, bottom right) of this configuration show that the algorithm is no longer able to reconstruct a reasonable image. It appears that data from other electrodes do not provide enough information for targets very near an affected electrode for adjacent drive current patterns.

Graphs of resolution vs. target position show that resolution becomes worse for all images calculated with missing data. However, resolution for $\mathbf{B}_{\sigma=\infty}$ is closer to $\mathbf{B}_0$ than $\mathbf{B}_Z$ in all cases for opposite drive, and for target positions < 0.7 for adjacent drive. For $\mathbf{B}_{\sigma=\infty}$ for adjacent drive and for targets near the affected electrode, resolution worsens in conjunction with an increase in position error.

Figure 6 illustrates the effect of electrode errors off axis with respect to the target position. A target at a radial position of 0.6 is imaged for affected electrodes E_0, E_1, E_2, E_3, and E_4 (columns from left to right). All images calculated with $\mathbf{B}_0$ are identical (since it does not assume electrode error). Images using $\mathbf{B}_{\sigma=\infty}$ show visually good images with few artefacts. Interestingly, the shape of the reconstructed image for E_1 and E_2 is noticibly elongated toward the affected electrode. All images reconstructed with $\mathbf{B}_Z$ show significant artefacts between the target position and the affected electrode, although the amplitude of these artefacts is less for opposite drive.

Figure 7 illustrates experimental data of ventilation and lung fluid instillation in a dog. From left to right, columns show images for measurement changes to due 700ml inspriation, 100ml fluid instillation, and both 700ml inspiration and 100ml fluid instillation. Rows of the image from top to bottom are reconstructed using $\mathbf{B}_0$, $\mathbf{B}_Z$, and $\mathbf{B}_{\sigma=\infty}$, respectively. A set of measurements was chosen where the signal from the affected electrode was of relatively low amplitude. This is somewhat unusual; in our experience, electrode errors typically completely mask the signal. For both $\mathbf{B}_Z$ and

$\mathbf{B}_{\sigma=\infty}$, the pattern of artefacts from the affected electrode has been eliminated. However, the ventilation signal is less visible in $\mathbf{B}_Z$ in the region of the lung closest to the affected electrode.

Discussion

Reconstruction of EIT images is sensitive to any errors and variability in electrode measurements. There are many sources of such variability; electrode readings can be falsified by subject movement and changes in posture, electronics noise and drift, and changes in electrode-skin impedance due to sweat or peripheral oedema. Contact may also be lost completely, due to improper placement, patient movement, or operator error. This paper considers the case where individual electrodes become detached or poorly connected, while the other electrodes continue to provide valid data. An image reconstruction methodology is proposed which calculates an image using the remaining "good" data.

Regularized image reconstruction is represented as $\hat{\mathbf{x}} = \left(\mathbf{H}^t \mathbf{R}_n^{-1} \mathbf{H} + \mathbf{R}_x\right)^{-1} \mathbf{H}^t \mathbf{R}_n^{-1} \mathbf{z}$, where R_x and R_n represent the *a priori* estimates of image and measurement noise cross correlations, respectively. Using this formulation, missing electrode data can be naturally modelled as infinite noise on all measurements using the affected electrodes. Position error and resolution were close (±10%) to the values calculated without missing electrode data as long as the target was further than 10% of the medium diameter from the affected electrode. When the target was close to the affected electrode, resolution worsens and position error increases, but the reconstructed image still visually appears to represent a reasonable "best effort". In comparison, simulations were made of the simple approach of setting measurements from affected electrodes to zero. Results for this approach showed significant artefacts at all target positions.

A modified reconstruction matrix, $\mathbf{B}_{\sigma=\sigma n^2}$, is introduced which models the affected electrodes as subject to an increased noise variance of σ_n^2. In most electrode error scenarios, little is known about the noise, and the most appropriate reconstruction matrix would use $\sigma=\infty$. However, in some specific cases, such as electronics hardware malfunction, there may be detailed information about the increased noise levels. In such a situation, using an appropriate noise model would allow improved image reconstruction, by still using (although to a lesser extent) the noisy data.

Since the proposed methodology is analysed using simulation data, it is natural to speculate on the importance of the details of the FEM and electrode models used. We feel that these details do not have a significant effect on the results, as a different FEM and electrode models (compound vs. simple) were used for the image reconstruction and simulation, and the observed effects did not show any significant dependence on these details of the models.

The methodology presented here may be readily incorporated into any EIT reconstruction algorithm based on regularization using a Jacobian. Most EIT algorithms (e.g. Polydorides and Lionheart, 2002, Vauhkonen *et al* 2001) do not explicitly incorporate a data noise term, such as the **W** matrix in the algorithm of Adler and Guardo (1996). For example, the EIDORS software toolbox expresses the core of the inverse solution as (`http://www.eidors.org`, version 1.01, file `inv_sol.m`, line 60):

```
sol = (J'*J + tfac*Reg'*Reg)\ (J' * (vi - voltage));
```

where `J` is the 3D Jacobian, `Reg` is the regularization matrix, `tfac` is the regularization parameter, and `vi - voltage` the data error at the current iteration. One could

introduce a **W** term into the calculation; however, a modification of the Jacobian will have the same effect. Note that this is only valid for $\sigma_n=\infty$, because the `J'*J` term would need to be modified differently from `J'*(vi-voltage)`, for other values of σ_n. The following pseudocode modifies the Jacobian to incorporate the electrode error information.

For each affected measurement *i*

For *j* = 1 to *M*

Set $\mathbf{J}_{i,j} = 0$

In terms of computational speed, the proposed approach adds virtually no extra time to the underlying algorithm; the only computational step is to loop through the Jacobian matrix to set certain elements to zero. In fact, by careful optimization, the pattern of zeros may be taken into account to speed up the calculation. While, conceptually, the framework introduced here is applicable to absolute imaging, it is possible that missing electrode data could cause an iterative solution to diverge. We have not been able to test this hypothesis is this report.

In conclusion, a methodology has been developed which is applicable to EIT data acquisitions in which individual electrodes produce erroneous data. The affected electrodes are identified, and this information is incorporated into a regularized image reconstruction algorithm. Applications of this technique to experimental data show promising results; artefacts are removed from the image without significant degradation in reconstructed image quality.

References

Adler A and Guardo R 1996a Electrical Impedance Tomography: Regularised Imaging and Contrast Detection *IEEE Trans. Medical Imag,* **15** 170-179

Adler A, Guardo R and Berthiaume Y 1996b Impedance Imaging of Lung Ventilation: Do we need to account for Chest Expansion? *IEEE Trans. Biomed. Eng.* **43** 414-421

Adler A, Amyot R, Guardo R, Bates J H T and Berthiaume Y 1997 Monitoring changes in lung air and liquid volumes with electrical impedance tomography *J. Appl. Physiol.* **83** 1762-1767

Al-Hatib F 1998 Patient-instrument connection errors in bioelectrical impedance measurement *Physiol. Meas.* **19** 285-296

Cook R D, Saulnier G J, Gisser D G, Goble J C, Newell J C and Isaacson D 1994 ACT3: a high-speed, high-precision electrical impedance tomograph *IEEE Trans. Biomed. Eng.* **41** 713-22

Frangi A F, Riu P J, Rosell J and Viergever M A 2002 Propagation of Measurement Noise Through Backprojection Reconstruction in Electrical Impedance Tomography *IEEE Trans. Med. Imaging* **21** 566-578

Geselowitz D B 1971 An Application of Electrocardiographic Lead Theory to Impedance Plethysmography *IEEE Trans. Biomed. Eng.* **18** 38-41

Guardo R, Boulay C, Murray B and Bertrand M 1991 An experimental Study in Electrical Impedance Tomography using Backprojection Reconstruction *Trans. Biomedical Eng.* **38** 617-627

Khambete N D, Brown B H and Smallwood R H 2000 Movement artefact rejection in impedance pneumography using six strategically placed electrodes *Physiol. Meas.* **21** 79-88

Lozano A, Rosell J and Pallás-Areny R 1995 Errors in prolonged electrical impedance measurements due to electrode repositioning and postural changes *Physiol. Meas.* **16** 121-130

Meeson S, Blott B, and Killingback A 1996 EIT data noise evaluation in the clinical environment, *Physiol. Meas.,* **17** (suppl.) A33-A38

Polydorides N and Lionheart W R B 2002 A Matlab toolkit for three-dimensional electrical impedance tomography: a contribution to the Electrical Impedance and Diffuse Optical Reconstruction Software project *Meas. Sci. Technol.* **13** 1871-1883

Swanson D K and Webster J G 1983 Errors in four-electrode impedance plethysmography *Med. Biol. Eng. Comput.* **21** 674-680

Vauhkonen M, Lionheart W R B, Heikkinen L M, Vauhkonen P J and Kaipio J P 2001 A Matlab package for the EIDORS project to reconstruct two-dimensional EIT images *Physiol. Meas.* 22 107-11

Wheeler J L, Wang W and Tang M 2002 A comparison of methods for measurement of spatial resolution in two-dimensional circular EIT images *Physiol. Meas.* **23** 169-176

Figure 1:

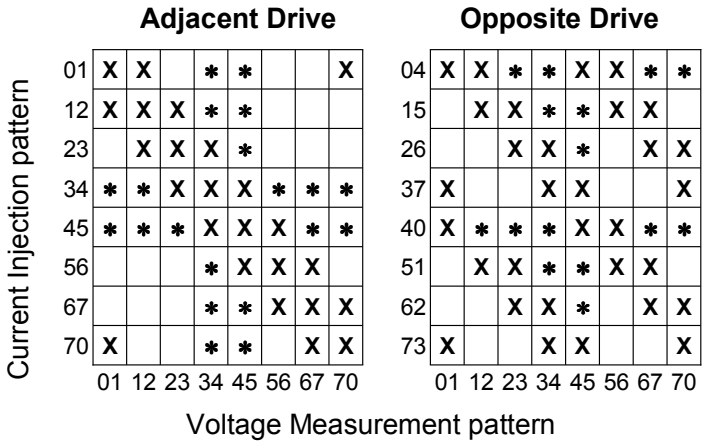

Caption:

Block diagram of measurement patterns for an 8 electrode EIT system, using adjacent drive (left) or opposite drive (right). Current injection patterns are shown on the vertical axis, where a current applied between electrodes 1 and 5 is indicated 15. Voltage measurement patterns are shown on the horizontal axis, where voltage measured between electrodes 1 and 2 is indicated 12. Voltage measurements are not taken at electrodes used for current injection; these positions are marked (**X**). If electrode 4 is disconnected, two columns and two rows of measurements become unavailable (∗).

Figure 2:

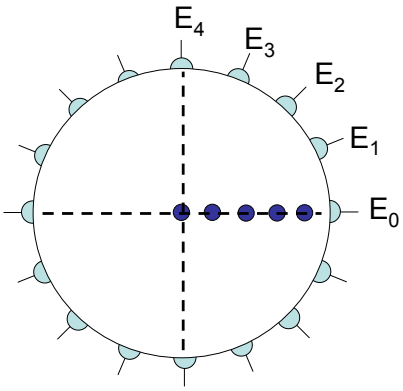

Caption:

Configuration of simulations. A 2D FEM is used to simulate a series of small non-conductive targets at radial positions of 0, 0.2, 0.4, 0.6, and 0.8. Electrodes E_0, E_1, E_2, E_3, and E_4 are used to simulate a disconnected electrode.

Figure 3A:

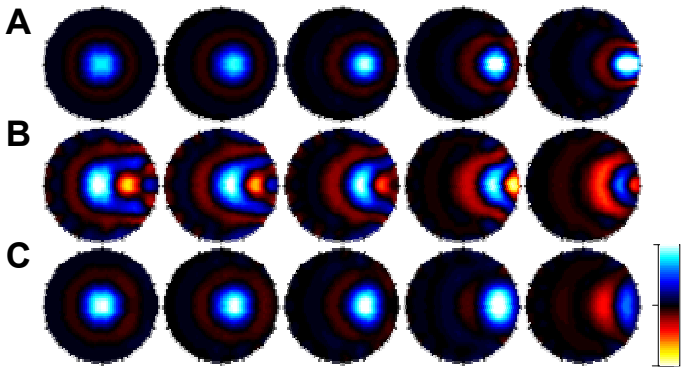

Figure 3B:

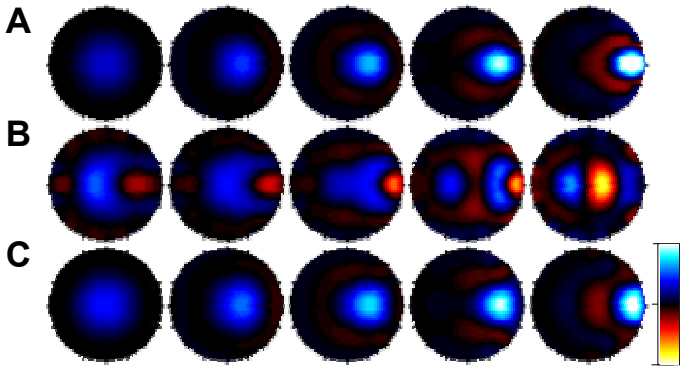

Caption:

Reconstructed images of log conductivity change as a function of target position for adjacent (figure 3A) and opposite (figure 3B) current patterns. Each row uses a different reconstruction matrix: $\mathbf{B}_0$ (no electrode errors, row A), $\mathbf{B}_Z$ (electrode error data set to zero, row B), and $\mathbf{B}_{\sigma=\infty}$ (electrode noise in regularized inverse, row C). Target radial positions are 0 (centre), 0.2, 0.4, 0.6 and 0.8 shown in each column from left to right. The affected electrode is E_0 (see figure 2). The colour scale is shown at lower right, with limits $\pm 1.9\times10^{-5}$ (figure 3A) and $\pm 1.6\times10^{-5}$ (figure 3B). Red corresponds to conductive, and blue to non-conductive conductivity changes.

Figure 4:

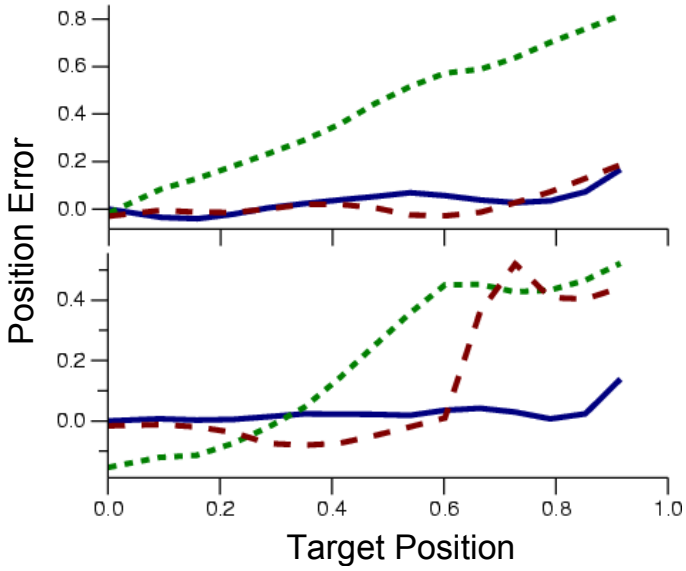

Caption:

Position error vs. target position for adjacent (lower) and opposite (upper) current patterns. Reconstruction matrices used are: $\mathbf{B}_0$ (no electrode errors, solid line), $\mathbf{B}_Z$ (electrode error data set to zero, dotted line), and $\mathbf{B}_{\sigma=\infty}$ (electrode noise in regularized inverse, dashed line)

Figure 5:

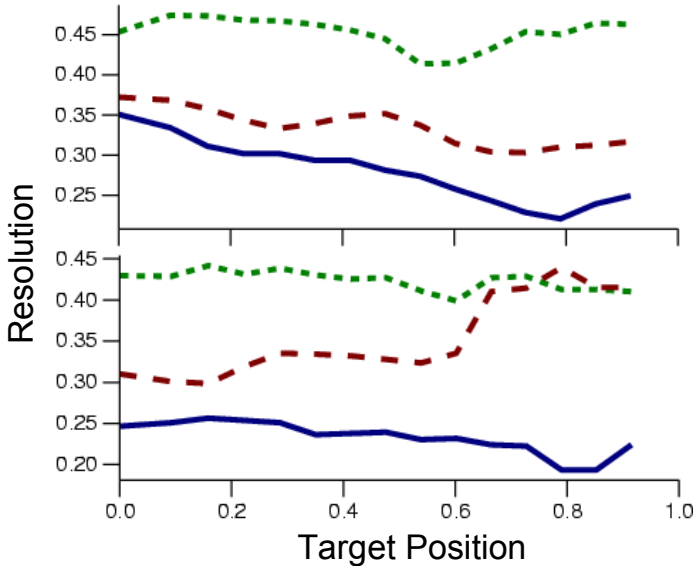

Caption:

Resolution vs. target position for adjacent (lower) and opposite (upper) current patterns. Reconstruction matrices used are: $\mathbf{B}_0$ (no electrode errors, solid line), $\mathbf{B}_Z$ (electrode error data set to zero, dotted line), and $\mathbf{B}_{\sigma=\infty}$ (electrode noise in regularized inverse, dashed line)

Figure 6A:

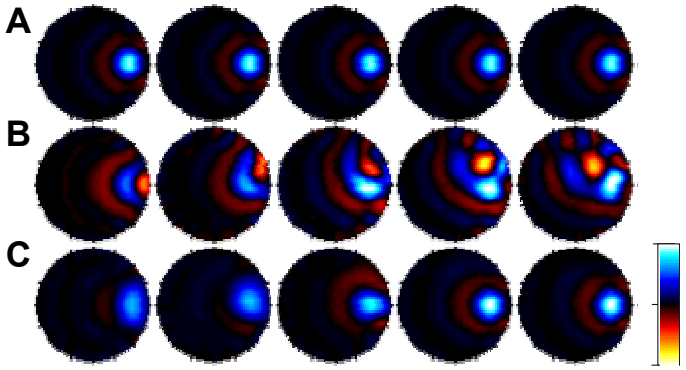

Figure 6B:

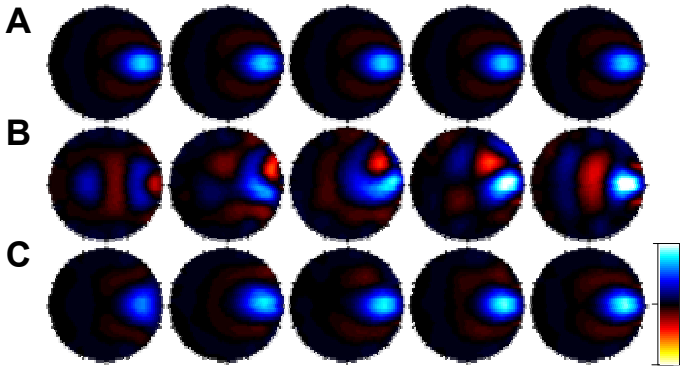

Caption:

Reconstructed images of log conductivity change as a function of affected electrode position for adjacent (figure 3A) and opposite (figure 3B) current patterns. Each row uses a different reconstruction matrix: $\mathbf{B}_0$ (no electrode errors, row A), $\mathbf{B}_Z$ (electrode error data set to zero, row B), and $\mathbf{B}_{\sigma=\infty}$ (electrode noise in regularized inverse, row C). All targets are at radial positions 0.6. Affected electrodes (see figure 2) E_0, E_1, E_2, E_3, and E_4 are shown in each column from left to right. The colour scale is shown at lower right, with limits $\pm 3.1\times10^{-5}$ (figure 3A) and $\pm 2.4\times10^{-5}$ (figure 3B).

Figure 7:

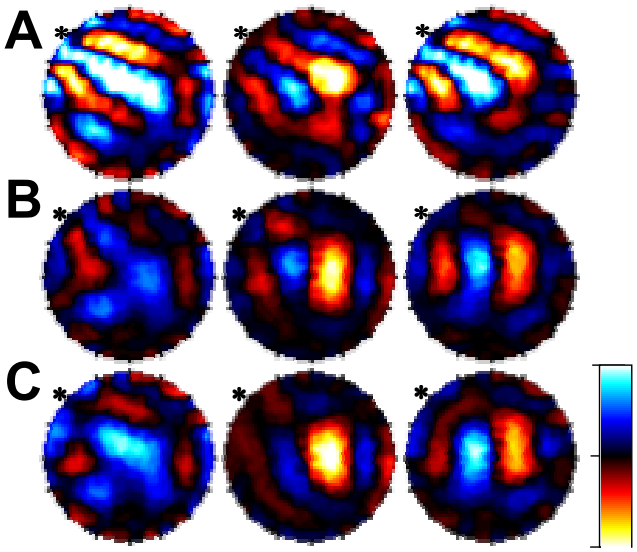

Caption:

Reconstructed cross sectional images of log conductivity change of ventilation and lung fluid instillation in a dog. Images are oriented so the top is ventral and image right side is subject right. From left to right, each column shows 700 ml inspiration, 100 ml fluid instillation into the right lung, and both 700 ml inspiration and 100 ml fluid. The affected electrode is indicated with ∗.Each row uses a different reconstruction matrix: $\mathbf{B}_0$ (no electrode errors, row A), $\mathbf{B}_Z$ (electrode error data set to zero, row B), and $\mathbf{B}_{\sigma=\infty}$ (electrode noise in regularized inverse, row C). Artefacts in row A are due to the presence of electrode errors, while the algorithm assumes there are none. The colour scale is shown at lower right, with limits ±0.15. Red corresponds to conductive, and blue to non-conductive conductivity changes.